Available online at www.sciencedirect.com
SCIENCE DIRECT
Journal of Photochemistry and Photobiology A: Chemistry 173 (2005) 56–63
Journal of Photochemistry and Photobiology A:Chemistry
www.elsevier.com/locate/jphotochem

Photocatalytic water decomposition for hydrogen production over silicotungstic acid–silica photocatalyst

The-Vinh Nguyen, Ki-Ju Kim, O-Bong Yang*

School of Environmental and Chemical Engineering, Center for Advanced Radiation Technology, Chonbuk National University, 664-14, 1st Street, Dukjin-Dong, Jeonju, Jeonbuk 561-756, Republic of Korea

Received 10 August 2004; received in revised form 27 November 2004; accepted 5 January 2005
Available online 30 January 2005

Abstract

A novel photocatalytic water decomposition to produce hydrogen was investigated over silicotungstic acid (SWA)–silica photocatalyst under UV irradiation. SWA–silica photocatalysts were prepared by impregnation of SWA on silica support as a function of solvent and mixing time of SWA and silica. The catalysts were characterized by BET surface area, X-ray diffraction, X-ray photoelectron spectroscopy, scanning electron microspectroscopy equipped with energy-dispersive X-ray spectroscopy and UV–vis diffuse reflectance spectroscopy. The charge transfer resistances of photocatalysts were analyzed by AC impedance measurement. The superior photocatalytic performance to produce hydrogen over SWA–silica is ascribed to the formation of secondary structure of SWA over silica support. Such a secondary structure results in the formation of bonding between SWA and support that is believed to be a dominant root for hydrogen evolution. The presence of SWA along with silica gives rise to the decrease in the charge transfer resistance, which is consistent with the superior performance of SWA–silica system.

Keywords: Silicotungstic acid; Silica; Photocatalytic water decomposition; AC impedance; Charge transfer

1. Introduction

Heteropolyacids (HPAs) are complex proton acids that incorporate polyoxometalate anions called as the primary structure of HPAs having metal–oxygen octahedral as the basic structural units [1]. The first characterized and the best known of these is the Keggin structure having the molecular formula $X^{n+}M_{12}O_{40}{}^{n-8}$, where X^{n+} is a central atom (Si^{4+}, P^{5+}, etc.), *n* is its oxidation state, and M is the metal ion (Mo^{6+}, W^{6+}, etc.). One can imagine the form of the Keggin anion as a sphere having a diameter of approximately 1 nm. In the solid state, Keggin structures act as anions in typical space lattices depending on the degree of hydration and the type of cation present, which is called as the secondary structure of HPAs.

HPAs, either in a homogeneous or a heterogeneous form, have been studied as catalysts [2,3], photocatalysts [4], stains for electron microscopy [5], and photo- and electrochromic materials [6] due to their unique redox activities and high electron densities [7]. However, in comparison with other semiconductor materials widely used in photocatalysis such as TiO_2, CdS, ZnO, FeO_x, etc., HPAs have received little attention because their excited-state lifetimes are on the picosecond time scale and so are too brief to engage in many chemical reactions [8]. In order to overcome this obstacle, immobilized HPAs have been introduced to enhance the "local" concentration of substrates to levels high enough that reactions may occur even on very short time scales [4]. On the other hand, by supporting HPAs on the solid surface, their specific surface areas are largely increased (BET specific surface areas of HPAs are lower than 10 m^2/g [9]) that may result in an increase in the catalytic activity of HPAs.

In this work, we report a novel concept: HPAs in combination with low-specific-surface-area silica could improve their photocatalytic activity under UV irradiation for water decomposition which has been extensively studied for production of

* Corresponding author. Tel.: +82 63 270 2313; fax: +82 63 270 2306.
E-mail address: obyang@chonbuk.ac.kr (O.-B. Yang).

1010-6030/$ – see front matter © 2005 Elsevier B.V. All rights reserved.
doi:10.1016/j.jphotochem.2005.01.003

hydrogen as an inexpensive source of clean energy [10–13]. To explain this concept, a unique photocatalytic reaction mechanism was discussed in conjunction with the structural properties of immobilized HPA and supports. A slurry of HPAs and silica in deionized water (S–HPA–silica) for photocatalytic water decomposition was also tested for comparison and elucidation of the reaction mechanism. Nitrogen adsorption, X-ray powder diffraction, XPS, SEM–EDS, UV–vis-DRS, and AC impedance were used to characterize the catalysts.

2. Experimental

2.1. Catalyst preparation

2.1.1. Conventional impregnation method

2.1.1.1. Method 1S (one step). Silica (naturally occurring microcrystalline silica, Sigma Chemical, denoted as SiO_2) and silica fumes (Sigma Chemical, named as SF2 and SF4) were employed as supports. Immobilized silicotungstic acid (Aldrich Chemical, designated as SWA) was prepared by impregnating the corresponding supports with 0.004 M aqueous solution of SWA to achieve a final loading of 5, 10, 15, 30, and 45 wt.%. The resulting slurries were evaporated immediately without any stirring under vacuum to dry and then calcined in static air at 350 °C for 4 h.

2.1.1.2. Method 2S (two steps). The suspension of corresponding supports and aqueous solution of SWA as stated in method 1S was mixed in the rotary evaporator at atmospheric pressure for 24 h and then the solvent was evacuated with a procedure same to that of method 1S.

2.1.1.3. Method 3S (three steps). The same suspension as above was stirred by using magnetic bar at room temperature for 24 h, then mixed in the rotary evaporator under atmospheric pressure for 24 h and finally evaporated under vacuum as stated in method 1S.

According to the preparation procedures described above, the contact time between SWA and supports obviously increases in the following order: 1S < 2S < 3S.

In order to investigate the effect of impregnation solvents on the properties of derived catalysts, water (W), methanol (M), ethanol (E), and *iso*-propanol (P) (with the polarity and surface tension in the sequence: water > methanol > ethanol > *iso*-propanol) were employed as impregnation solutions.

2.1.2. Equilibrium technique

The solvent of 1/1 mixture (volumetric) of deionized water and ethanol was used to make the SWA solution with a concentration of 120 g W/l solvent. The preparation of the catalysts by equilibrium technique was performed as follows at 20 °C: the slurry of 5 g support and 20 ml of SWA solution was stirred for 72 h to attain equilibrium; the slurry was centrifuged and filtrated; the solid sample was calcined at 200 °C for 3 h. The obtained solid was washed with water under vigorous stirring for three times; finally the catalyst was calcined at 200 °C for 3 h, which denoted as SWA/SiO_2-Eq.

The acronyms of SWA-immobilized catalysts can be explained as an example of SWA(15)/SiO_2–1S–W: SWA stands for silicotungstic acid. Next numeral represents weight percentage of SWA immobilized on SiO_2 support. The subsequent numeral and letter depict the impregnation method, 1S. The final character indicates the solvent employed in impregnation solution, water (W).

2.2. Catalyst characterization and water decomposition experiment

The catalysts were characterized by nitrogen adsorption (Micromeritics ASAP 2100) to measure the BET surface areas, pore sizes and pore volumes, X-ray diffraction (XRD, Rigaku, Cu Kα radiation), X-ray photoelectron spectroscopy (XPS, Perkin-Elmer PHI 5400, Al Kα radiation), and scanning electron spectroscopy (SEM, Hitachi S-4700) equipped with energy-dispersive X-ray elemental analysis system (EDS, Horiba EMAX). The absorption of bare SWA over support was determined by analyzing the effluent solution of corresponding catalyst with ultraviolet–visible spectrometer (UV–vis, HP-8452A). The bandgap energy was measured using UV–vis diffuse reflectance spectra (UV–vis-DRS, Shimadzu UV-2401).

The setup for AC impedance measurement was consisted of a lock-in amplifier (EG&G 5210) coupled with a potentiostat (EG&G 273) and software (EG&G M398). The working electrodes used for AC impedance measurement were prepared by coating method. Photocatalysts were ground in mortar and pestle before mixing and sonicating with deionized water (10 min) to obtain coating suspensions (0.8 M). After coating and drying (in static air at room temperature) on a disk glassy carbon electrode (MF-2012, BAS) with the surface area of 7.065×10^{-6} m^2, a solution of Nafion (5%, containing 15–20% water, Aldrich Chemical) as a binder was covered over the layer of photocatalyst. The derived electrodes were dried in an oven at 100 °C for 30 min. The characterization of electrodes was carried out in an electrochemical cell with 0.1 M $HClO_4$ electrolyte, using anodes of photocatalysts as the working electrodes, a Pt wire as the counter electrode and a Ag/AgCl/3 M NaCl electrode as the reference electrode.

The photocatalytic water decomposition was carried out in an inner irradiation quartz cell reaction system under UV irradiation. In the outer Pyrex cell, 700 ml of an aqueous slurry containing 1 g of a fine powder photocatalyst was well mixed by a magnetic bar during the reaction. The reaction cell was purged by bubbling with ultrapure nitrogen until oxygen-free. A high-pressure mercury lamp (450 W) in the inner quartz cell was used as a UV light source. The average reaction temperature was 296 ± 3 K. For the analysis of reaction products under UV irradiation, 500 μl of gas was sampled with a gas-tight syringe. The amounts of evolved

Table 1
Structural properties of various catalysts

Catalysts	BET specific surface area (m^2/g)	Pore volume (cm^3/g)	Pore size (nm)
SiO_2	6.30	2.70×10^{-2}	16.87
SWA	11.24	1.61×10^{-2}	11.55
SF2	268	–	–
SF4	352	–	–
SWA(5)/SiO_2–2S–E	6.94	1.91×10^{-2}	15.08
SWA(5)/SiO_2–1S–W	5.65	2.14×10^{-2}	17.64
SWA(5)/SF2–1S–W	255	–	–
SWA(5)/SF4–1S–W	335	1.58	36.68

H_2 and O_2 were quantitatively measured by a gas chromatograph equipped with a thermal conductivity detector and a molecular sieve 5A column (30 m × 0.35 mm × 50.0 μm film thickness, HP; N_2 carrier).

3. Results and discussion

3.1. Characterization

The structural properties of various catalysts are presented in Table 1. The order of BET specific surface areas of catalysts is SWA(5)/SF4–1S–W > SWA(5)/SF2–1S–W ≫ SWA(5)/SiO_2–1S–W. The BET specific surface areas and pore sizes of SiO_2-based catalysts are almost similar. Meanwhile, the pore sizes of SF4 (fumed silica)-based catalysts are two times larger than those of SiO_2-based samples. Fig. 1 presents the pore size distribution of bare SiO_2, SWA(5)/SiO_2–1S–W, and SWA(5)/SiO_2–2S–E. The pore volumes of SWA-loaded SiO_2 catalysts are lower than that of bare SiO_2 at any given pore sizes, which is ascribed to the low pore volume of bare SWA compared to that of bare SiO_2 as shown in Table 1. It is noteworthy that the peaks at ca. 3.7 and 10 nm are observed on bare SiO_2 and SWA(5)/SiO_2–2S–E but not on SWA(5)/SiO_2–1S–W, which can be interpreted by the fact that 3.7 and 10 nm pores of SiO_2 on SWA(5)/SiO_2–1S–W are filled with the secondary structure of SWA. Meanwhile, isolated primary SWA which is dispersed on SiO_2 is probably predominant on SWA(5)/SiO_2–2S–E catalyst.

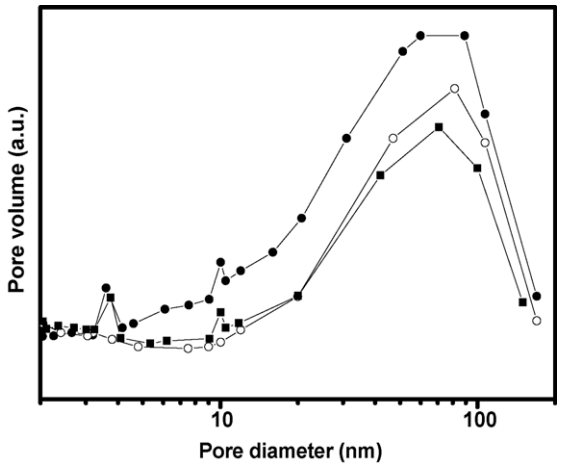

Fig. 1. Pore size distribution of bare SiO_2 (●), SWA(5)/SiO_2–1S–W (○) and SWA(5)/SiO_2–2S–E (■).

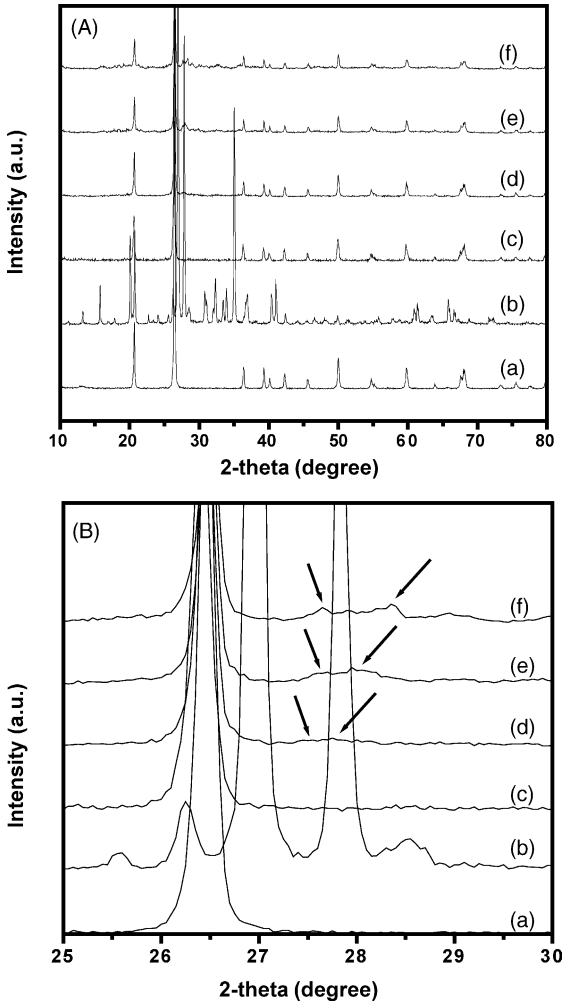

Fig. 2. X-ray diffraction patterns over 2θ range of 10–80° (A) and 25–30° (B) of bare SiO_2 (a), bare SWA (b), SWA(5)/SiO_2–1S–W (c), SWA(15)/SiO_2–1S–W (d), SWA(30)/SiO_2–1S–W (e), and SWA(45)/SiO_2–1S–W (f). The arrows show the characteristic peaks of immobilized SWA.

Fig. 2 shows the XRD patterns of the catalysts with different compositions of SWA over SiO_2. SWA(5)/SiO_2–1S–W does not reveal any diffraction peaks of crystalline heteropolyacid (26.95° and 27.85° of 2θ). In addition, the intensity of SiO_2 crystallite peak (26.45° of 2θ) is gradually decreased as increasing the composition of SWA while the peaks of SWA crystallites is not significantly appeared even the composition of SWA as high as 45 wt.%. It has been reported in a recent literature that up to 40–45 wt.% of SWA could be entrapped within the silica structure which was ascribed to the huge surface thereof [14]. In XRD patterns the characteristic peaks of SWA (26.95° and 27.85° of 2θ, with a shoulder shape) of immobilized SWA gradually shift to higher 2θ values relative to pure SWA which has dom-

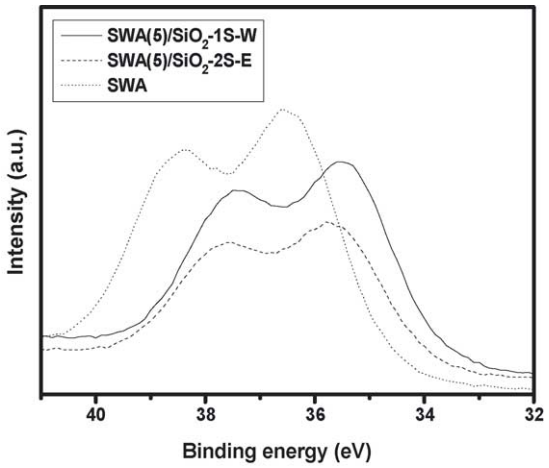

Fig. 3. XPS W $4f_{7/2}$ for the catalysts, bare SWA, SWA(5)/SiO_2–1S–W, and SWA(5)/SiO_2–2S–E.

inantly secondary structure. In other words, the higher the SWA loading, the more the Keggin units, $SiW_{12}O_{40}^{4-}$ rather than the secondary structures, $(H_4SiW_{12}O_{40}{\cdot}xH_2O)_n$ over the supports.

Fig. 3 depicts the XPS spectra of bare SWA, SWA(5)/SiO_2–1S–W, and SWA(5)/SiO_2–2S–E and the data are shown in Table 2. The symmetric peaks of O 1s are observed at 532.50 and 532.60 eV for SWA(5)/SiO_2–1S–W and SWA(5)/SiO_2–2S–E, respectively. These can be identified as oxygen in OH^- groups on the catalysts [15]. The peaks of 36.6, 35.60, and 35.80 eV are corresponded to W $4f_{7/2}$ doublet of bare SWA, SWA(5)/SiO_2–1S–W, and SWA(5)/SiO_2–2S–E, respectively. It has been reported that the binding energies related to W^{6+}, W^{5+}, and W^{4+} are 35.6, 34.5, and 33.5 eV on the WO_x/ZrO_2 catalysts, respectively [16]. Accordingly, the binding energy difference of ca. 1 eV between bare SWA and SWA(5)/SiO_2–1S–W and SWA(5)/SiO_2–2S–E can be due to the transition from W^{7+} to W^{6+} of partial content of SWA supported on SiO_2. This partial substitution of W=O by W–O bond may result from the formation of interaction between the secondary structure of SWA and SiO_2. About 0.2 eV lower binding energy of W $4f_{7/2}$ in SWA(5)/SiO_2–1S–W than in SWA(5)/SiO_2–2S–E suggests that the interaction between the secondary structure of SWA and SiO_2 is stronger in the former than in the latter. The contribution of W $4f_{7/2}$ in SWA(5)/SiO_2–1S–W is found substantially higher than that of W $4f_{7/2}$ in SWA(5)/SiO_2–2S–E. This result indicates that the amount of SWA on exterior surface over SWA(5)SiO_2–1S–W is much larger than that over SWA(5)/SiO_2–2S–E, because XPS data mainly reveal the exterior surface information rather than the interior texture properties of the samples.

Table 3
Atomic composition data by EDS analysis for various catalysts

Catalyst	Atomic composition (%)	
	O	Si
SiO_2	66.9	33.1
SWA(5)/SiO_2–1S–W	73.2	26.8
SWA(5)/SiO_2–1S–E	70.5	29.5
SWA(5)/SiO_2–2S–E	67.5	32.5

Elemental analysis of the catalysts was carried out by SEM–EDS (Table 3). EDS analysis was scanned to obtain the average elemental composition on the surface of catalysts with a 0.5 μm^2 analysis window (scanned area) coupled with SEM images. Tungsten element is not detected by EDS due to very low atomic content. Only silicon and oxygen peaks are appeared in EDS spectra in which the oxygen atoms result from SWA and SiO_2. Table 3 shows the atomic composition of O and Si by EDS analysis. The empirical atomic composition of O in pure SiO_2 (66.9%) is a little higher than its theoretical one (66.7%), which is attributed to the adsorption of water on the SiO_2 surface. On the other hand, the theoretical atomic composition of O in SWA(5)/SiO_2–X–Y (X = 1S and 2S, Y = W and E) is 67.1% in which all of Keggin units are supposed to be fixed on the exterior surface of SiO_2. However, the atomic compositions of O in the catalysts are much higher than the theoretical value. These results are attributed to the relative absorption of water vapor on the Keggin units and SiO_2 surface. Nevertheless, such errors could cancel one another while comparing the experimental data. On SWA(5)/SiO_2–1S–W, the dispersion of SWA on the exterior surface of SiO_2 was found to be higher than the others.

In order to elucidate the electronic properties of SWA-based catalysts, the electrochemical system employed in this study for AC impedance characterization was simulated by an equivalent simple circuit as shown in the inset of Fig. 4. The constituents of the circuit for the simulation are considered as follows: the resistance of electrolyte solution (R_S), the charge transfer resistance at the electrolyte/catalyst film interface and the catalyst film/glassy carbon electrode interface along with the conduction in catalyst film (R_{ct}), and space charge capacitance (C_{sc}) [17]. The AC impedance plots were recorded over frequency range from 0.015 to 10 kHz with AC amplitude of 5 mV. Fig. 4 shows the plots of bare SiO_2, bare SiO_2 in SWA solution (an equivalent of a slurry of 1.0 g

Table 2
Bandgap energies and XPS data of catalysts

Catalysts	Bandgap (eV)	Energy (eV)/at.%			
		O 1s	C 1s	Si 2p	W 4f
Bare SWA	3.4	531.8/44.45	284.6/40.21	102.6/1.70	36.6/13.63
SWA(5)/SiO_2–1S–W	3.4	532.5/45.94	284.6/31.36	103.4/21.62	35.6/1.08
SWA(5)/SiO_2–2S–E	3.4	532.6/45.83	284.6/31.31	103.6/22.09	35.8/0.77

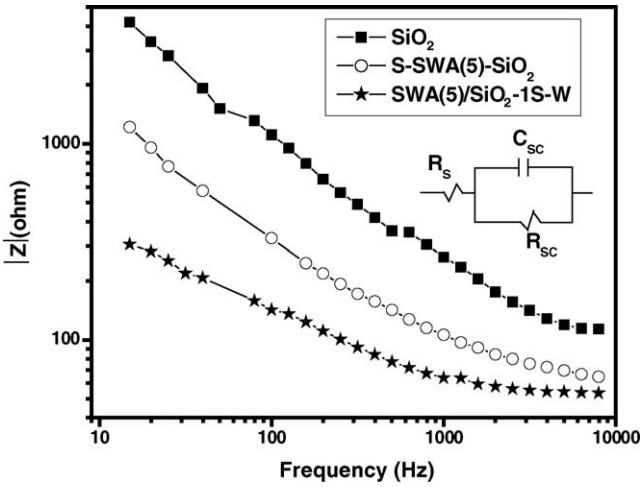

Fig. 4. Bode $|Z|$ plots of the catalysts from 0.015 to 10 kHz under irradiated state. The inset shows an equivalent simple circuit modeling the experimental cell.

of SWA (5 wt.%) and SiO_2) denoted as S–SWA(5)–SiO_2 and SWA(5)/SiO_2–1S–W under UV illumination. At any given frequencies, the AC impedances of catalysts are SWA(5)/SiO_2–1S–W < S–SWA(5)–SiO_2 ≪ bare SiO_2. This result implies that the presence of SWA in SiO_2 strongly affects the resistance of catalysts. In other words, SWA in combination with SiO_2 significantly improves the density of photo-excited electrons under illumination, resulting in the decrease of impedance.

3.2. Photocatalytic water decomposition

Table 4 shows the performance of photocatalytic water decomposition. SWA as a homogenous photocatalyst shows negligible photoactivity to decompose water into H_2 and O_2 under UV illumination. It has been reported due to very low specific surface area of HPAs (<10 m^2/g) and too brief excited lifetime of electrons under illumination as discussed in Section 1. In addition, SiO_2 also shows very low photocatalytic activity for water decomposition. However, the slurry of silica and SWA solution, S–SWA(5)–SiO_2 in 700 mL pure water evolves hydrogen as high as 10.9 μmol/h under UV irradiation. By a UV–vis analysis of the effluent solution of aqueous slurry of S–SWA(5)–SiO_2, a significant amount of SWA (ca. 29%) in the solution was adsorbed on SiO_2 right after a mixing. Accordingly, the drastic performance improvement of S–SWA(5)–SiO_2 might results from the adsorbed SWA on the support, which acts as an essential promoter for the photocatalytic water decomposition. Furthermore, when SWA is immobilized on SiO_2 with appropriate conditions like SWA(5)/SiO_2–1S–W, the resulting catalyst shows significantly improved performance up to 32.8 μmol H_2/h, which is three times higher than that of S–SWA(5)–SiO_2. These results are well agreement with the resistance trend in AC impedance spectroscopy: bare SiO_2 ≫ S–SWA(5)–SiO_2 > SWA(5)/SiO_2–1S–W, suggesting that the lower the resistance, the higher the photocatalytic activity.

Table 4
Performance of photocatalytic water decomposition for hydrogen production over various catalysts

Catalyst	H_2 evolution[a] (μmol/h)
SWA	0.837
SiO_2	0.625
S–SWA(5)–SiO_2	10.85
SWA(5)/SiO_2–1S–W	32.79
SWA(15)/SiO_2–1S–W	10.85
SWA(45)/SiO_2–1S–W	3.21
SWA(5)/SF2–1S–W	15.24
SWA(5)/SF4–1S–W	10.45
SWA(5)/SiO_2–2S–W	6.99
SWA(5)/SiO_2–3S–W	9.47
SWA(5)/SiO_2–1S–M	11.98
SWA(5)/SiO_2–1S–E	9.33
SWA(5)/SiO_2–1S–P	10.92
SWA/SiO_2–Eq	7.02
SWA(5)/SiO_2–2S–M	9.47
SWA(5)/SiO_2–2S–E	18.67
SWA(5)/SiO_2–2S–P	10.05

[a] Stoichiometric ratio of H_2 and O_2 was approximately observed on all of SWA–silica systems; the value was obtained by averaging out at 10-h run.

It was well known that the catalytic activity of supported HPAs depends on several parameters such as carrier type, HPA concentration, and pre-treatment conditions [9]. The immobilized SWA catalyst prepared with water as solvent and 1S mode shows the highest photocatalytic activity for hydrogen evolution compared to that prepared with ethanol as solvent and either 1S or 2S mode (Table 4). In the case of water solvent and 1S mode to prepare the immobilized SWA, SWA might be aggregated on the exterior surface of support due to the high surface tension of water and short contact time in 1S method between SWA and support. This condition is favorable for the formation of secondary structure of SWA. Meanwhile, with a longer mixing time of 2S mode and a lower surface tension of ethanol solvent, SWA prefers to form a monolayer of isolated Keggin anions over the exterior surface of support or migrate into the pores thereof. Since there are countercations (H^+, H_3O^+, $H_5O_2^+$, etc.) and hydration water, the secondary structure of SWA is dominantly bonded with silica support under calcination compared to the Keggin unit as depicted in Fig. 5a. For the formation of the interaction between SWA and the surface of silica, the substitution of W=O by W–O bond should occur as observed by XPS data (Table 2) and depicted in Fig. 5a.

From the fact that higher hydrogen production on SWA(5)/SiO_2–1S–W than that on SWA(5)/SiO_2–2S–E, the secondary structure of SWA is advantageous to the photocatalytic water decomposition to produce hydrogen. As shown in Table 4, the photocatalytic activity is increased as decreasing the SWA loading due to the suitable condition to form the secondary structure in low loading of SWA. Because the same concentration of SWA solution was employed for all of impregnation methods, the higher the SWA load-

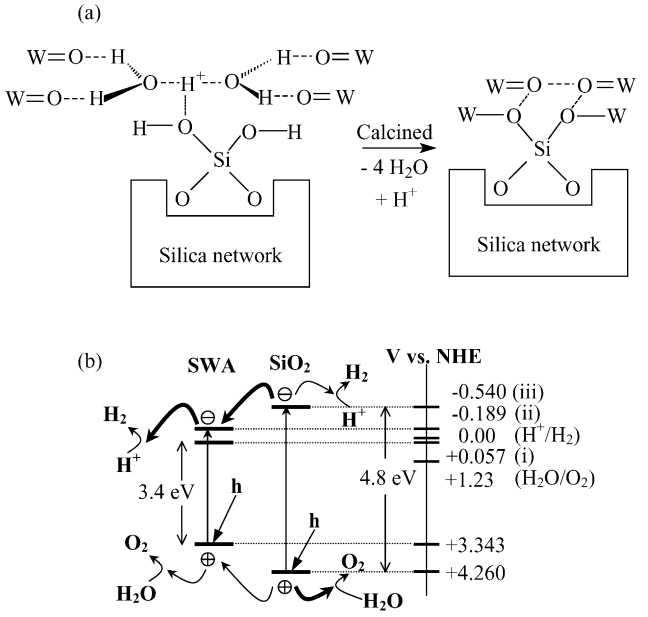

Fig. 5. Schematic illustration of the formation of SWA (secondary structure)–silica linkage (a) and water decomposition mechanism over immobilized SWA (b). (i) The reduction potential for the first step of SWA ($SiW_{12}O_{40}^{4-/5-}$); (ii) the reduction potential for the second step of SWA ($SiW_{12}O_{40}^{4-/6-}$); (iii) the reduction potential of the photoactive site of silica (≡Si–O•). The thick arrows mean the dominant pathways for hydrogen and oxygen evolution. W=O represents the primary structure of SWA. The diagram is not in scale.

ing, the longer the contact time between SWA and supports during impregnation processes. Such a long contact time in SWA(45)/SiO_2–1S–W may be favorable to form the highly dispersed SWAs in which they exist as Keggin units. Furthermore, it is well known that excess dopant acts as the electron–hole recombination centers on the derived photocatalyst [18]. Accordingly, very low photocatalytic performance of SWA(45)/SiO_2–1S–W (even much less than that of S–SWA(5)–SiO_2) could be attributed to not only less amount of the secondary structure of SWA but also the electron–hole de-excitation sites. As shown in Table 1, the higher the pore size and specific surface area of supports (the pore size and specific surface area: SF4 > SF2 > SiO_2), the lower the photocatalytic activity of derived catalysts. High specific surface area and pore size of support give rise to the high dispersion of SWA over it, resulting in the formation of monolayer of isolated Keggin anions. This result suggests that the reaction of water decomposition for hydrogen takes place in the bulk of the secondary structure of SWA rather than on the well-dispersed Keggin units. Also, this result is consistent with the fact that the secondary structure of SWA may act as the essential active sites for the photocatalytic water decomposition. It is noteworthy that the photocatalytic activities of most catalysts though prepared under different pre-treatment conditions (including SWA/SiO_2-Eq) are same magnitude to that of S–SWA(5)–SiO_2 to some extent. These results are probably ascribed to the facts that low surface tension of methanol, ethanol, and *iso*-propanol as well as long contact time between SWA and support seem to suppress the formation of the secondary structure of SWA on support.

On the basis of the characterization results and photocatalytic activities of SWA–SiO_2 catalysts, the silica support appears to be photoactive and engage in the charge transfer process with immobilized SWA. The charge transfer process could explain the substantial decrease in the resistance of immobilized SWA as well as the improvement of its density of excited electrons under illumination. The stronger the interaction between SWA and support, the more efficient the charge transfer between them, which is responsible for the improvement of photocatalytic performance of immobilized SWA. Mesoporous and amorphous silica have been reported as photoactive supports [19,20]. The photoactive sites on these supports are generated by dehydroxylation of surface-isolated hydroxyl groups as shown in Scheme 1 [19].

It is noteworthy that the photoactive sites on bare silica as reported in the literature [19,20] are generated through evacuation at high temperature, which is not the case of this present study. This is well supported by the fact that bare SiO_2 is almost inert under UV illumination to produce hydrogen (Table 4). Nevertheless, in conjunction with SWA through the W–O–Si bonding, the photoactive property of SiO_2 support may be generated as illustrated in Scheme 2. Under UV illumination, the charge transfer from O to W in SWA results in electron–hole separation as represented in Scheme 2a [21]. Simultaneously, non-bridging oxygen hole center (≡Si–O•) would be the photoactive site by the charge transfer of Si → O• in the W–O–Si linkage under irradiation (Scheme 2b) [19]. Accordingly, we can propose the overall mechanism in Scheme 2c where the generated hole on Si is transferred to surrounding oxygen [19]. The proposed mechanism in Scheme 2 is consistently supported by the photocatalytic activities of catalysts and the AC impedance data.

The first and second reduction steps of SWA were reported at +0.057 and −0.189 V versus NHE at pH 0, respectively [21,22], in which only the latter is responsible for the reduction of water to produce hydrogen. The valence band of SiO_2 is +4.26 V (versus NHE at pH 0) [23] while the photoactive site (≡Si–O•) can be excited un-

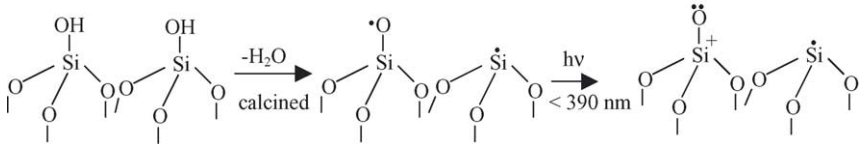

Scheme 1.

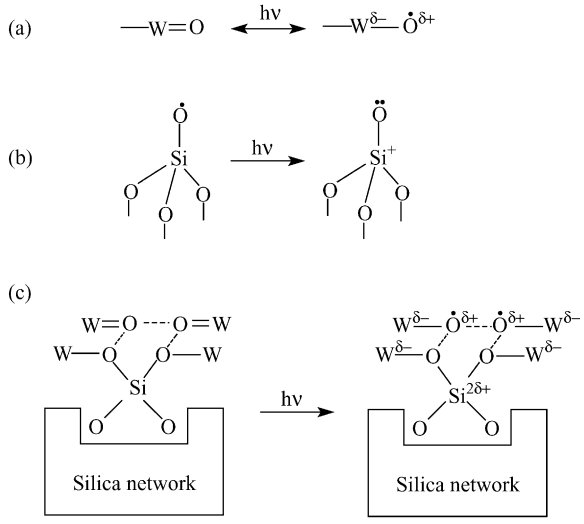

Scheme 2.

der the light at 4.8 eV [19]. From the UV–vis-DRS absorption spectra shown in Fig. 6, the onset of absorption for SWA(5)/SiO_2–1S–W and SWA(5)/SiO_2–2S–E occur at ca. 365 nm. Therefore, the bandgap energies of SWA(5)/SiO_2–1S–W and SWA(5)/SiO_2–2S–E are calculated as ca. 3.4 eV (Table 2) (by the equation, eV ≈ 1239.95/λ, where λ is the wavelength in nm at the onset of absorption spectrum). The band edges of SWA and SiO_2 are also depicted in Fig. 5b. Based on this band edge structure, the synergistic performance of SWA–SiO_2 system could be well explained by the charge transfer mechanism: under UV irradiation, photo-excited electrons from the photoactive sites of SiO_2 are transferred to the conduction band of SWA to produce hydrogen. Since the conduction band and valence band of SWA are lower and higher than the deep traps and the valence band of SiO_2, respectively, photo-excited electrons and holes would tend to recombine easily provided that the transfer speeds of electrons and holes from SiO_2 to SWA were almost same. However, the cooperative motion of the holes is an inherently slower process than that of the electrons, which is ascribed to the much higher mobility of the latter than the former. As a result, the electrons transferred from SiO_2 to SWA predominantly reduce H^+ to produce H_2 before they recombine with the holes which are moving from SiO_2 to SWA or directly taking part in the oxygen formation reaction on the SiO_2 surface. Accordingly, the effective reduction of water for the production of hydrogen might be taken place by the electron moved from SiO_2 to SWA. Meanwhile oxygen seems to be mainly evolved by the holes on SiO_2 itself rather than the holes transferred from SiO_2 to SWA, resulting in the improvement of photocatalytic performance due to the reverse flows of electrons and holes as shown in Fig. 5b. A similar mechanism has been reported in our recent study for RuS_2/TiO_2–SiO_2 system [24].

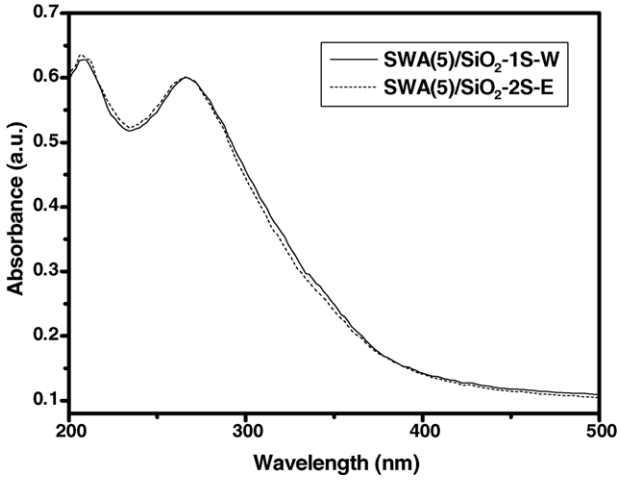

Fig. 6. UV–vis-DRS of SWA(5)/SiO_2–1S–W and SWA(5)/SiO_2–2S–E.

4. Conclusions

A novel photocatalytic water decomposition to hydrogen was observed over SWA–SiO_2 system. The composition of SWA on silica, impregnation method, and impregnation solvent are essential factors to form the secondary structure of SWA over silica. SWA/SiO_2 prepared by 1S method and water solvent shows the highest water decomposition photoactivity, which is attributed to the formation of strong bonding between the secondary structure of SWA and silica. This strong bonding of SWA and silica results in the decrease of the resistance of SWA/silica photocatalyst that is ascribed to the charge transfer phenomenon. The role of photoactive sites in SiO_2 as a donor source for hydrogen formation and that of SWA as an inhibitor of the recombination of photo-excited electrons and holes are appreciable and responsible for the superior photocatalytic performance of SWA–SiO_2 system.

Acknowledgements

The authors acknowledge the financial support from the Korea Industry Technology Foundation (MOCIE) by the program of Human Resources Development for Regional Innovation and the Center for Ultramicrochemical Process Systems (CUPS) sponsored by Korea Science and Engineering Foundation (KOSEF).

References

[1] M.T. Pope, Heteropoly and Isopoly Oxometalates, Springer, Berlin, 1983.
[2] N. Mizuno, M. Misono, Chem. Rev. 98 (1998) 199–218.
[3] M. Sadakane, E. Steckhan, Chem. Rev. 98 (1998) 219–238.
[4] R.R. Ozer, J.L. Ferry, J. Phys. Chem. B 106 (2002) 4336–4342.
[5] J.F. Keana, M.D. Ogan, Y. Lu, M. Beer, J. Varkey, J. Am. Chem. Soc. 107 (1985) 6714–6715.
[6] T. Yamase, Chem. Rev. 98 (1998) 307–326.

[7] R.C. Schroden, C.F. Blanford, B.J. Melde, B.J.S. Johnson, A. Stein, Chem. Mater. 13 (2001) 1074.
[8] D.C. Duncan, T.L. Netzel, C.L. Hill, Inorg. Chem. 34 (1995) 4640.
[9] I.V. Kozhevnikov, Chem. Rev. 98 (1998) 175.
[10] Z. Zou, J. Ye, K. Sayama, H. Arakawa, Nature 414 (2001) 625.
[11] T. Takada, A. Tanaka, M. Hara, J.N. Kondo, K. Domen, Catal. Today 44 (1998) 19.
[12] C.T.K. Thaminimulla, T. Takata, M. Hara, J.N. Kondo, K. Domen, J. Catal. 196 (2000) 362.
[13] J. Ye, Z. Zou, H. Arakawa, M. Oshikiri, M. Shimoda, A. Matsushita, T. Shishido, J. Photochem. Photobiol. A 148 (2002) 79.
[14] P. Staiti, S. Freeing, S. Hocevar, J. Power Source 79 (1999) 250–255.
[15] R. Dziembaj, A. Malecka, Z. Piwowarska, A. Bielanski, J. Mol. Catal. A: Chem. 112 (1996) 423–430.
[16] M. Occhiuzzi, D. Cordischi, D. Gazzoli, M. Valigi, P.C. Heydorn, Appl. Catal. A 269 (2004) 169–177.
[17] The space charge capacity of the catalyst film (C_{sc}) is in series with that of the Helmholtz capacity (C_H). Thus the total capacity is given by: $1/C = 1/C_{sc} + 1/C_H$. Since $C_H \gg C_{sc}$ (the capacity of Helmholtz is ca. 10 μF/cm^2), the measured $-Z_{im}$ ($-Z_{im} = 1/\omega C$) is that of the space charge layer.
[18] M.I. Litter, J.A. Navío, J. Photochem. Photobiol. A 98 (1996) 171.
[19] Y. Inaki, H. Yoshida, T. Yoshida, T. Hattori, J. Phys. Chem. B 106 (2002) 9098–9106.
[20] H. Yoshida, T. Tanaka, M. Yamamoto, T. Yoshida, T. Funabiki, S. Yoshida, J. Catal. 171 (1997) 351–357.
[21] A. Hiskia, A. Mylonas, E. Papaconstantinou, Chem. Soc. Rev. 30 (2001) 66.
[22] A. Troupis, A. Hiskia, E. Papaconstantinou, Appl. Catal. B: Environ. 42 (2003) 312.
[23] G.A. Zacheis, K.A. Gray, P.V. Kamat, J. Phys. Chem. B 105 (2001) 4719.
[24] T.-V. Nguyen, S.S. Kim, O.-B. Yang, Catal. Commun. 5 (2004) 59–62.